

On the X-ray Image of The Crab Nebula: Comparison with Chandra Observations

Shinpei SHIBATA¹, Haruhiko TOMATSURI¹,
Makiko SHIMANUKI¹, Kazuyuki SAITO¹, Koji MORI²

¹Department of Physics Yamagata University, Yamagata 990-8560, JAPAN,

²Department of Astronomy and Astrophysics, 525 Davey Laboratory,
The Pennsylvania State University, University Park, PA 16802, USA

in original form 2003 June 23, revised 5 August, accepted 25 August 2003 for MNRAS

Abstract

An axisymmetric model for the Crab Nebula is constructed to examine the flow dynamics in the nebula. The model is based on that of Kennel and Coroniti (1984), although we assume that the kinetic-energy-dominant wind is confined in an equatorial region. The evolution of the distribution function of the electron-positron plasma flowing out in the nebula is calculated. Given viewing angles, we reproduce an image of the nebula and compare it with Chandra observation.

The reproduced image is not a ring-like but rather 'lip-shaped'. It is found that the assumption of toroidal field does not reproduce the Chandra image. We must assume that there is disordered magnetic field with an amplitude as large as the mean toroidal field. In addition, the brightness contrast between the front and back sides of the ring cannot be reproduced if we assume that the magnetization parameter σ is as small as $\sim 10^{-3}$. The brightness profile along the semi-major axis of the torus is also examined. The non-dissipative, ideal-MHD approximation in the nebula appears to break down.

We speculate that if the magnetic energy is released by some process that produce turbulent field in the nebula flow and causes heating and acceleration, e.g. by magnetic reconnection, then the present difficulties may be resolved (i.e. we can reproduce a ring

image, and a higher brightness contrast). Thus, the magnetization parameter σ can be larger than previously expected.

stars: pulsars: general – ISM: individual: Crab Nebula

1 Introduction

A standard picture of the Crab Nebula was given by Kennel and Coroniti (KC; 1984). According to their picture, a super-fast magnetohydrodynamic wind, which is generated by the central pulsar, terminates at a shock, with the nebula identified as a postshock flow shining in synchrotron radiation. The central cavity of the nebula is occupied by the unseen wind. The shock is supposed to occur at the standing inner wisp.

The KC model is very successful explaining the synchrotron luminosity, spectrum and frequency-dependent size of the nebula. An important conclusion of the KC model is that the energy of the wind is conveyed mostly by kinetic energy in the bulk motion of the plasma. Because the energy flux is in the form of an electromagnetic field at the base of the wind, this means that the efficiency of the wind acceleration is extremely high; KC found it to be 99.7%.

The principal parameters of the pulsar wind are (1) its luminosity L_w , (2) the Lorentz factor γ_w of

the bulk flow and (3) the ratio σ of the electromagnetic energy flux to the kinetic energy flux, which is referred to as the magnetization parameter. L_w is essentially the spin-down luminosity $\approx 5 \times 10^{38}$ erg s $^{-1}$. The remaining two parameters, γ_w and σ , together with the nebula pressure P_N , or equivalently the equipartition field $B_{eq} = \sqrt{4\pi P_N}$, determine the overall synchrotron spectrum. Conversely, the synchrotron spectrum tells us about the parameters. Given the synchrotron luminosity of 2×10^{37} erg s $^{-1}$, the nebula size of ~ 1 pc, and the peak and turn-off synchrotron spectrum energies of 2 eV and 10^8 eV, respectively, one finds $\gamma_w = 3.3 \times 10^6$, $\sigma = 3.8 \times 10^{-3}$, and $B_{eq} = 0.38$ mG. This result can be obtained even with an order-of-magnitude estimate (Shibata, Kawai and Tamura 1998). More rigorous fitting of the observed spectrum of the whole nebula gave similar values (e.g., KC, Atoyan and Aharonian 1996). The field strength has been confirmed by observations of inverse Compton emission in the TeV band (Weekes et al. 1989; Hillas et al. 1998). Thus, the dominance of the kinetic energy of the wind seems very firm.

From a theoretical point of view, however, the smallness of σ , or in other words dominance of the kinetic energy, is a mystery. No wind theory has been able to explain how such a high efficiency of acceleration is achieved.

Chandra observation clearly shows a disk-jet structure and moving wisps with seeds of $\sim 0.45c$ (Mori 2002), where c is the speed of light. Because the KC model is spherically symmetric and steady, it may seem insufficient to understand the highly structured and dynamical nature seen by Chandra. However, the basic idea that a kinetic dominant wind shocks and shines seems still firm and convincing. One may assume that the equatorial wind has different parameters than the polar wind. Such a latitude dependence of the wind parameters may suffice to explain the apparent disk-jet structure although how such a latitude dependence is made is not known.

In this paper, we suggest that high spatial resolution of Chandra affords a chance to examine the assumptions which were made in the KC model but have yet to be checked. Among the assumptions, the ideal-MHD condition (no dissipation) and toroidal

field approximation are of particular importance. If these assumptions are not adequate, the past conclusion of small σ may need to be reconsidered.

We model the nebula in 3-dimensions based on the KC picture and reproduce an image, which can be compared with the Chandra observation (Mori 2002) is made. We shall show that a considerable change to the KC picture is required to reproduce the Chandra image. In this paper, we suggest that disordered magnetic field in the nebula is needed. Some process which converts magnetic energy into thermal and kinetic energy, such as magnetic reconnection, may take place in the nebula. In a subsequent paper, spatially-resolved X-ray spectra will be described and compared with Chandra results.

2 A 3D Model

We postulate that the nebula flow obeys the KC steady solution and do not solve the dynamics. The properties of the KC flow are summarized as follows. If σ is much less than unity as was suggested, the speed of the flow is $\sim (1/3)c$ just after the shock and decreases rapidly with distance from the pulsar R as $V \propto R^{-2}$; because the flow is subsonic, the pressure and density n are roughly uniform as for adiabatic expansion such that the mass conservation, $nR^2V \approx \text{const.}$ (implying a decrease of the flow velocity). Due to deceleration, the magnetic field accumulates and is amplified according to the frozen-in condition, $B \propto r$. Once the magnetic field grows as large as the equipartition field, the magnetic pressure becomes important in the flow dynamics. As a result, the flow speed saturates. This takes place where the nebula is brightest (at $\sim (3\sqrt{\sigma})^{-1}$ shock radii). The smaller σ , the larger and brighter the nebula. The smallness of σ is then required to explain the luminosity and the extent of the nebula. The indicated flow speed is small if σ is small: $V/c \sim 3\sigma$. It is notable here that the above flow dynamics depends on the assumption of the ideal-MHD condition.

The KC model is spherically symmetric and obviously inadequate to account for the observed morphology. We therefore restricted ourselves to an equatorial region of the KC spherical model with half

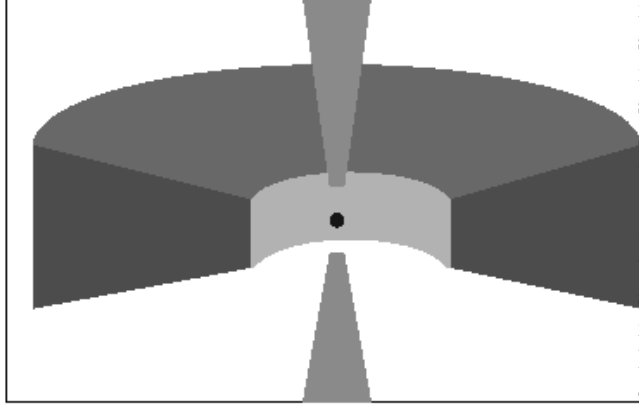


Figure 1: The three-dimensional structure we assumed for reproduction of image. The spherical flow by Kennel and Coroniti (1984) is picked up for the disk and polar flows.

width of $\Theta_{eq} \sim 10^\circ$ and cut the intermediate latitude regions out, such that the disk may be reproduced in an image (see Fig. 1). Although we assume a polar flow by leaving the polar region with a semi-opening angle of $\Theta_{pol} \sim 10^\circ$ for reproduction of the jet image, this is just in an artist's spirit, and we do not provide any analysis of the polar jets in this paper.

Our kinematic scheme to reproduce images of the nebula is made so that different types of the flow dynamics can be applied in the future; i.e., for a given velocity field, we trace a fluid element and associated particle distribution function according to the Lagrangian view of fluid.

Given the radial velocity field $V(t, R)$ as a function of time and radial distance from the pulsar, the position of the fluid element, the toroidal magnetic field, and the proper density are respectively obtained from

$$\frac{DR}{Dt} = V, \quad (1)$$

$$\frac{D}{Dt}(\ln B) = -\left(\frac{V}{R} + \frac{\partial V}{\partial R}\right), \quad (2)$$

$$\frac{D}{Dt}(\ln n) = -\frac{D}{Dt}(\ln \Gamma) - \left(\frac{2V}{R} + \frac{\partial V}{\partial R}\right), \quad (3)$$

where t is the observer's time and $\Gamma = (1 - V^2/c^2)^{-1/2}$

is the Lorentz factor of the flow. We use the KC solution, which is given analytically, for the velocity field. Although the KC solution does not include synchrotron losses, its effect on V is supposed to be small because synchrotron losses are about 10% of the kinetic energy of the flow.

For the energy distribution of the particles, we again invoke the KC picture: a power law distribution is built up immediately after the shock, and the shock-accelerated particles simply lose their energy in the postshock flow by adiabatic and synchrotron losses. We trace the energy ϵ (normalized by mc^2) of each particle in a fluid frame by

$$\frac{D}{Dt'}(\ln \epsilon) = \frac{1}{3} \frac{D}{Dt'}(\ln n) + \frac{1}{\epsilon} \left(\frac{d\epsilon}{dt'} \right)_{\text{loss}}, \quad (4)$$

where

$$-\left(\frac{d\epsilon}{dt'} \right)_{\text{loss}} = \frac{4}{3} \sigma_T c \epsilon^2 U_{\text{mag}}, \quad (5)$$

and the magnetic energy density, $U_{\text{mag}} = B^2/8\pi\Gamma^2$, is measured in the proper frame, and σ_T is the Thomson cross section. The proper time t' is related to t by $Dt/Dt' = \Gamma$.

The distribution function is defined by

$$dn = f(t, R; \epsilon, \theta) \sin \theta d\theta d\varphi d\epsilon, \quad (6)$$

where θ is the pitch angle with respect to the local field and φ is the azimuth. Note that the distribution function is defined in the flow proper frame. We assume that the postshock distribution follows a power law with index p (≥ 1) in between the minimum energy ϵ_{min} and the maximum energy ϵ_{max} , and it is isotropic such that

$$f_i(\epsilon_i) = \frac{K}{4\pi} n_i \epsilon_i^{-p}, \quad (7)$$

where the suffix 'i' indicates 'injection' at the postshock region, and the normalization is given by

$$K = \begin{cases} \frac{(p-1)\epsilon_{\text{min}}^{(p-1)}}{1 - (\epsilon_{\text{min}}/\epsilon_{\text{max}})^{p-1}} & p \neq 1 \\ \frac{1}{\ln(\epsilon_{\text{max}}/\epsilon_{\text{min}})} & p = 1 \end{cases} \quad (8)$$

and $n_i = \iiint f_i(\epsilon) \sin \theta d\theta d\varphi d\epsilon$ gives the postshock proper density. ϵ_{max} is assumed to be a maximum

attainable value, eB_2R_s/mc^2 , where R_s is the shock distance from the pulsar, and B_2 is the postshock field. ϵ_{\min} is determined so that the pressure calculated from f_i satisfies the shock jump condition.

We solve (4) numerically for a sample of particles in a given fluid element, and thereby we obtain ϵ as a function of ϵ_i and t . Then we calculate distribution functions from

$$f(\epsilon(R)) = \frac{n}{n_i} f_i(\epsilon_i) \frac{d\epsilon_i}{d\epsilon}. \quad (9)$$

For steady state models, integration for a single fluid element gives distribution functions in the whole nebula.

It is obvious that the above kinematic scheme can be easily generalized for non-steady and non-radial flow, which can be obtained by numerical MHD simulations.

3 Reproduction of the Nebula Image

3.1 Synchrotron Specific Emissivity

Once the evolution equations (1)-(4) are solved, and the distribution function is obtained by (9), it is straight forward to get volume emissivity, which is integrated to give a nebula image.

Since the nebula flow is relativistic, a Lorentz transformation is applied between the flow proper frame and the observer's frame (or rather the pulsar frame, in which the pulsar is at rest). Let us denote the 4-vector of a synchrotron photon by $(\omega/c, \mathbf{k})$ in the observer's frame and $(\omega'/c, \mathbf{k}')$ in the proper frame. If the ideal-MHD condition $\mathbf{E} + \mathbf{V} \times \mathbf{B}/c = 0$ holds in the nebula flow, the transformation of the electromagnetic field is simpler:

$$\mathbf{E}' = 0, \quad (10)$$

$$\mathbf{B}'_{\parallel} = \mathbf{B}_{\parallel} = (\mathbf{V} \cdot \mathbf{B})\mathbf{V}/V^2, \quad (11)$$

$$\mathbf{B}'_{\perp} = \mathbf{B}_{\perp}/\Gamma = (\mathbf{B} - \mathbf{B}_{\parallel})/\Gamma, \quad (12)$$

where the primes indicate the quantities in the flow frame and \parallel and \perp are based on the directed of the

flow velocity \mathbf{V} . There is no electric field in the plasma flow frame.

The spectral power of a relativistic particle with pitch angle θ (the angle of the particle motion to the local magnetic field in the proper frame) is

$$\mathcal{P}_{\text{s1}}(\omega', \epsilon, \theta) = 2\sigma_T c U_{\text{mag}} \epsilon^2 \sin^2 \theta \mathcal{S}(\omega'; \omega_c). \quad (13)$$

For the monochromatic approximation, we use $\mathcal{S}(\omega'; \omega_c) = \delta(\omega' - \omega_c)$, and for the relativistic approximation,

$$\mathcal{S}(\omega'; \omega_c) = \frac{9\sqrt{3}}{8\pi\omega_c} F\left(\frac{\omega'}{\omega_c}\right) \quad (14)$$

where $F(x) = x \int_x^{\infty} K_{\frac{5}{3}}(\xi) d\xi$, and

$$\omega_c = \frac{3e|\mathbf{B}'|\epsilon^2 \sin \theta}{2mc} \quad (15)$$

is the critical frequency. The synchrotron power of a single particle is strongly beamed within a width of $\sim \epsilon^{-1}$. Therefore, the emission into a frequency interval $d\omega'$ and in a solid angle $d\Omega'$ directed toward the observer is given by

$$j_{\omega'}(\theta) d\omega' d\Omega' = \int_0^{\infty} \mathcal{P}_{\text{s1}}(\omega', \theta, \epsilon) f(\epsilon, \theta) d\epsilon d\Omega' d\omega', \quad (16)$$

where θ is given by $\cos \theta = \mathbf{n}' \cdot \mathbf{B}'/|\mathbf{B}'|$, and \mathbf{n}' is the unit vector directing to the observer in the proper frame. Below, \mathbf{n} indicates the observer's direction in the observer's frame.

For the link between the proper frame and the observer's frame, we include the Doppler effects,

$$\omega = \frac{\omega'}{\Gamma(1 - \beta\mu)} \quad \text{and} \quad \mu = \frac{\mu' + \beta}{1 + \beta\mu'}, \quad (17)$$

where $\mu = \mathbf{n} \cdot \hat{\mathbf{V}}$ and $\mu' = \mathbf{n}' \cdot \hat{\mathbf{V}}$. The unit vector of the flow direction is denoted by $\hat{\mathbf{V}}$. The transformation between the received power dP_r and the emitted power dP' (Rybicki & Lightman 1979) is given by

$$\frac{dP_r}{d\Omega d\omega} = \Gamma^3 (1 + \beta\mu')^3 \frac{dP'}{d\Omega' d\omega'} = \frac{1}{\Gamma^3 (1 - \beta\mu)^3} \frac{dP'}{d\Omega' d\omega'} \quad (18)$$

where the Doppler effect (17) has been taken into account. Finally the Lorentz contraction is $dN = \Gamma f(\epsilon, \theta) d\Omega' d\epsilon$, where N is the number density in the observer's frame. Thus the emissivity in the observer's frame becomes

$$j_\omega(\mathbf{n}) = C \int \mathcal{P}_{s1}(\omega', \theta, \epsilon) f(\epsilon, \theta) d\epsilon, \quad (19)$$

where

$$C = \Gamma^4 (1 + \beta \mu')^3 = \frac{1}{\Gamma^2 (1 - \beta \mu)^3}. \quad (20)$$

3.2 Viewing Angle

In order to specify the viewing angle of the observer, we relate the 'observer's coordinate' $\mathbf{X} = (X, Y, Z)$, where $+X$ directed toward the observer and $+Z$ directed toward north on the sky, to the 'nebula coordinate' $\mathbf{x} = (x, y, z)$, where the z -axis coincides with the symmetry axis of the nebula which is believed to be the rotation axis of the pulsar. We use 48° and 28° as the position angle and the inclination angle of the symmetry axis, respectively.

An image of the nebula is obtained by

$$I_\omega(Y, Z) = \int_{-\infty}^{\infty} j_\omega(X, Y, Z, \mathbf{n}) dX. \quad (21)$$

3.3 Summary of the procedure

For a given observation frequency, the integration (21) is done numerically for each 'pixel' at (Y, Z) . The integrand is calculated as follows:

1. Given $\mathbf{X} = (X, Y, Z)$ and ω ,
2. transformation from the observer's coordinates to the nebula coordinates is done; for the position, $(X, Y, Z) \rightarrow (x, y, z)$, and also for the components of the observer's direction, $\mathbf{n} = (1, 0, 0) \rightarrow \mathbf{n} = (n_x, n_y, n_z)$.
3. The flow velocity $\mathbf{V}(R)$ and the magnetic field $\mathbf{B}(R)$ at the point are obtained by using the KC solution. Note that the velocity and the magnetic field are respectively radial and azimuthal in the 'nebula coordinate'.

4. The observation frequency, the direction and the local magnetic field are transformed into those in the flow frame: $\omega \rightarrow \omega'$, $\mathbf{n} \rightarrow \mathbf{n}'$, $\mathbf{B} \rightarrow \mathbf{B}'$.
5. The pitch angle of the particles directed toward the observer is obtained.
6. Regarding the distribution function at (x, y, z) , the emissivity in the flow frame is calculated (we use the monochromatic approximation).
7. Finally, the emissivity is converted to the volume emissivity $j_\omega(\mathbf{n})$ at (X, Y, Z) in the observer's frame by multiplying by the Doppler factor C .

4 Results

One may expect a ring-like structure in the reproduced image, such as observed with Chandra (see the top panel of Fig. 2), since we have assumed that the flow is restricted within a disk. The expected radius of the ring will be $\sim 1/3\sqrt{\sigma}$ (about 6 shock radii for $\sigma = 0.003$), at which point the nebula brightens due to the amplified magnetic field. However, what we have is not a ring-like but is rather a 'lip-shaped' image shown in the bottom panel of Fig. 2. At the north-east and south-west corners of the expected ellipse (ring), the pitch angles of the particles directed toward us are small, and therefore the surface brightness is reduced. This effect combined with the central cavity yields an image which is 'lip-shaped'. The smallness of pitch angle actually has two effects. One is that the single-particle emissivity is proportional to $\sin^2 \theta$, which is small. The other is due to number of contributing particles. For a given observation frequency, the energy of the particles radiating at the frequency is higher for smaller pitch angles, so that the number of particles contributing to the frequency is smaller because of the negative slope of the distribution function.

Another important point to consider is the intensity ratio between the front and back sides of the ring. We obtain a value of 1.3, but observed value is ~ 5 (Pelling et al. 1987, Willingale et al., 2001). The weak contrast is caused by deceleration of the nebula flow (i.e. the smallness of σ). Mori et al. (2003)

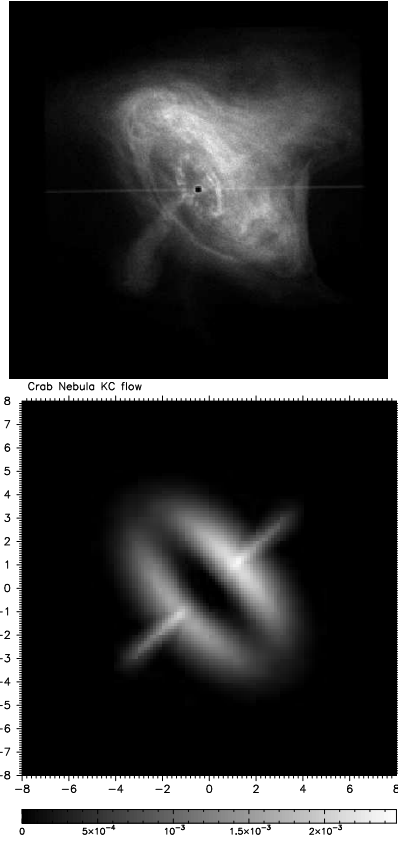


Figure 2: The Chandra image (top) and a reproduced image (bottom), where we assume a postshock flow with $\sigma = 0.003$ by Kennel and Coroniti (1984) but the flow is assumed to be restricted within an equatorial region. For the bottom image, the gray scale is in units of $0.016 \text{ erg s}^{-1} \text{ cm}^{-2} \text{ str eV}$.

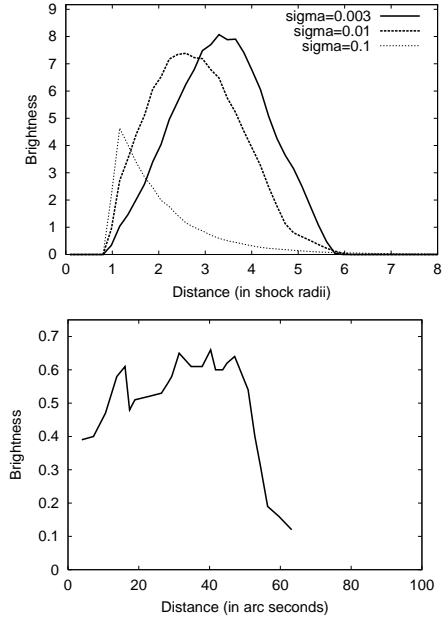


Figure 3: Surface brightness along the semi-major axis of the torus in the north-east direction. The upper panel shows the calculation with different σ 's while the lower panel is measured from the Chandra observation (Mori 2002). The distance is in units of the shock radius (which is supposed to be about $13'' - 14''$) for the model, and in arc seconds for the observation. The brightness is in units of $10^6 \text{ erg s}^{-1} \text{ cm}^{-2} \text{ str}^{-1} \text{ eV}^{-1}$ for the model and in counts $\text{s}^{-1} \text{ arcsec}^{-2}$ for the observation.

suggest that the ratio is about 3 with Chandra. This value is still incompatible with the KC picture. As long as the intensity contrast is attributed to Doppler boosting, such a weak contrast is unavoidable in the frame work of the KC model.

How surface brightness changes with distance from the shock depends on σ . Mori (2002) also measured the surface brightness along the semi-major axis of the torus, from which Doppler boosting should not affect the brightness. This result (bottom panel of Fig. 3) is compared with the present model (top panel of Fig. 3), for which we provide curves of varying

σ . The present model does not reproduce the first peak in the observation, which corresponds to the inner ring. However, it is notable that the brightness distribution of the inner ring is similar to that for the $\sigma = 0.1$ model. The location of synchrotron burn off is reproduced by the $\sigma = 0.01$ model. Finally, we point out that the surface brightness decreases much faster with distance in the observation than in the model.

As indicated by the 'lip-shaped' image, the absolute value of the surface brightness is much less than observed along the semi-major axis. Because the reproduced image includes only the disk component, to which we restricted ourselves (rather than assuming the spherical KC model), the X-ray luminosity of the reproduced image is also smaller than the observation. For the image in Fig. 2, we use parameters given by KC: $L_w = 5 \times 10^{38} \text{ erg s}^{-1}$, $R_s = 3 \times 10^{17} \text{ cm}$, $\gamma_w = 3 \times 10^6$, and $p = 3$. In this case, we have $\nu L_\nu \sim 10^{36} \text{ erg sec}^{-1}$ at 1 keV.

5 Discussion

Applying the KC model, we reconstruct an X-ray image which is found to be inconsistent with the Chandra image. Owing to a pure toroidal field and uniform pitch angle distribution, the reproduced image is not ring-like but 'lip-shaped'. Furthermore, the surface brightness contrast between the front and back sides of the ring is much less than the observed. The weak contrast is simply due to the smallness of σ , by which the postshock flow slows down quickly after the shock. The assumptions of the toroidal field and the smallness of σ are thus found to be incompatible with the observation.

If we assume isotropic emission in the proper frame such as is expected in a turbulent field, then the ring-like structure is reproduced as shown in Fig. 4. As would be expected, we find that such a turbulent component must be at least comparable to the mean toroidal field in order to reproduce the ring image. Although an another solution can be to adopt a contrived pitch angle distribution, we think this is unlikely. The image in Fig. 4 is produced in the following way: (1) assume the magnetic field is random

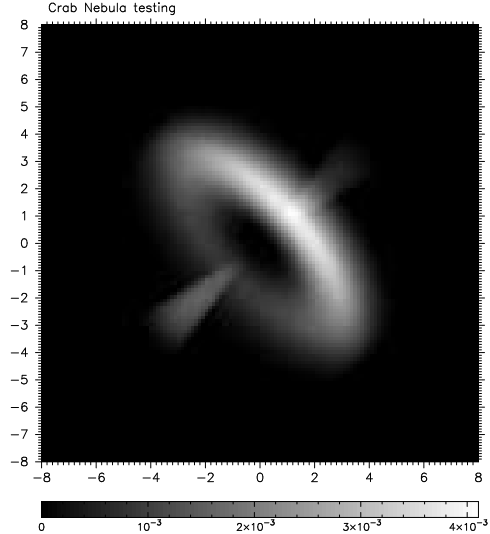


Figure 4: An image reproduced with assumptions of a turbulent field and a high speed flow. See text in detail.

so that the emissivity is isotropic in the proper frame; (2) set the flow velocity to be $0.2c$ by hand, ignoring the flow dynamics; (3) let the distribution function and the field strength follow the KC model. Thus, the random field and the fast flow are essential to reproduce the image.

With this practice, we suggest that the nebula field is far from pure toroidal, but rather is disordered. Such a disordered field can be produced by magnetic reconnection or some instability of the toroidal flux tubes. If there is dissipation of the magnetic field, the flow dynamics is importantly changed, as is the flow speed. Even if the value of σ , which is defined in the wind, is not small, dissipation in the nebula flow causes deceleration and brightening. In this sense, σ is effectively small so that the luminosity of the nebula will be explained as the KC model. But, such a simple heating may not always be good for explaining the surface brightness contrast because of the deceleration. Recently, Komissarov & Lyubarsky (2003) provide an MHD simulation for the Crab Nebula, suggesting a complicated flow pattern and a high speed flow such that the brightness contrast can be repro-

duced. Three dimensional motions associated with magnetic energy conversion in the nebula will considerably change the picture of the nebula. Numerical simulations for the nebular flow is of particular importance in the future study. As noted, the present image-production scheme will be easily extended to combine with such numerical results.

A model explaining the Chandra observation may be constructed if we assume a larger σ and a subsequent magnetic energy conversion into heat and plasma kinetic energy, such as magnetic reconnection, in the nebula flow. Suppose σ is rather large, then the postshock flow must be faster. The inner ring is formed at the shock. The brightness distribution will be similar to that of $\sigma = 0.1$ in Fig. 3. As the flow proceeds outward, the magnetic energy conversion takes place (accelerating and heating the flow). This causes the second brightening. Subsequently, the synchrotron burn-off provides the outer boundary of the torus. The Doppler effect will cause a higher brightness contrast. We note that the smallness of σ is not obvious if non-ideal-MHD is introduced in the nebula flow.

The above hypothesis explains the disk formation. Obliqueness of the pulsar causes a series of current sheets with an interval of the light cylinder radius ($\sim 10^8$ cm) in the equatorial region. If the current sheets dissipate in the nebula, the synchrotron emission brightening is restricted in the equatorial region, where reconnection takes place. The appearance of pulsar nebulae should depend on obliqueness of individual pulsars. High obliqueness results in a thick disk and a high efficiency of synchrotron luminosity, while near-alignment causes a faint nebulae.

The possibility of a dissipative process in the nebula may be examined more rigorously with spatially-resolved spectra, for which we will compare the model and the observation in a subsequent paper.

Acknowledgments

The authors thank F. E. Bauer for careful review of the manuscript. This work was supported by JSPS KAKENHI (C), 15540227. K. M. is supported by the JSPS postdoctoral fellowship for research abroad.

References

- [1] Atoyan, A. M. & Aharonian, F. A. 1996, MNRAS 278 525
- [2] Hillas A. M. et al., 1998, ApJ 503, 744
- [3] Kennel, C. F. & Coroniti, F. V. 1984, ApJ 283 694
- [4] Kennel, C. F. & Coroniti, F. V. 1984, ApJ 283 710
- [5] Komissarov S.S., Lyubarsky Y.E., 2003, astro-ph/0306162
- [6] Mori, K., 2002 PhD thesis, Osaka University
- [7] Mori, K., Burrows D. N., Hester, J. J., Shibata, S., Pavlov, G., Tsunemi, H., 2003, in preparation.
- [Pelling et al.(1987)] Pelling, R. M., Paciesas, W. S., Peterson, L. E., Makishima, K., Oda, M., Ogawara, Y., & Miyamoto, S. 1987, ApJ, 319, 416
- [8] Rybicki G. B., Lightman A. P., 1979, Radiative Processes in Astrophysics, Wiley & Sons, New York
- [9] Shibata S., Kawai N., Tamura K., 1998, in "Neutron Stars and Pulsars", eds. N. Shibasaki, N. Kawai, S. Shibata, T. Kifune, Universal Academy Press, Tokyo Japan, p. 457
- [10] Weekes T. C., 1989, ApJ 342, 379
- [Willingale et al.(2001)] Willingale, R., Aschenbach, B., Griffiths, R. G., Sembay, S., Warwick, R. S., Becker, W., Abbey, A. F., & Bonnet-Bidaud, J.-M. 2001, AA, 365, L212